JCI The Journal of Clinical Investigation

Cardiomyocyte PDGFR-β signaling is an essential component of the mouse cardiac response to load-induced stress

Vishnu Chintalgattu, … , Mark L. Entman, Aarif Y. Khakoo

J Clin Invest. 2010;120(2):472-484. https://doi.org/10.1172/JCI39434.

Research Article **Cardiology**

PDGFR is an important target for novel anticancer therapeutics because it is overexpressed in a wide variety of malignancies. Recently, however, several anticancer drugs that inhibit PDGFR signaling have been associated with clinical heart failure. Understanding this effect of PDGFR inhibitors has been difficult because the role of PDGFR signaling in the heart remains largely unexplored. As described herein, we have found that PDGFR-β expression and activation increase dramatically in the hearts of mice exposed to load-induced cardiac stress. In mice in which *Pdgfrb* was knocked out in the heart in development or in adulthood, exposure to load-induced stress resulted in cardiac dysfunction and heart failure. Mechanistically, we showed that cardiomyocyte PDGFR-β signaling plays a vital role in stress-induced cardiac angiogenesis. Specifically, we demonstrated that cardiomyocyte PDGFR-β was an essential upstream regulator of the stress-induced paracrine angiogenic capacity (the angiogenic potential) of cardiomyocytes. These results demonstrate that cardiomyocyte PDGFR-β is a regulator of the compensatory cardiac response to pressure overload–induced stress. Furthermore, our findings may provide insights into the mechanism of cardiotoxicity due to anticancer PDGFR inhibitors.

Cardiomyocyte PDGFR-β signaling is an essential component of the mouse cardiac response to load-induced stress

Vishnu Chintalgattu,[1] Di Ai,[1] Robert R. Langley,[2] Jianhu Zhang,[1] James A. Bankson,[3] Tiffany L. Shih,[1] Anilkumar K. Reddy,[4] Kevin R. Coombes,[5] Iyad N. Daher,[1] Shibani Pati,[6] Shalin S. Patel,[1] Jennifer S. Pocius,[4] George E. Taffet,[4] L. Maximillian Buja,[7] Mark L. Entman,[4] and Aarif Y. Khakoo[1]

[1]Department of Cardiology, [2]Department of Cancer Biology, and [3]Department of Imaging Physics, University of Texas MD Anderson Cancer Center, Houston, Texas, USA. [4]Department of Medicine, Baylor College of Medicine, Houston, Texas, USA. [5]Department of Bioinformatics and Computational Biology, University of Texas MD Anderson Cancer Center, Houston, Texas, USA. [6]Center for Translation Injury Research and [7]Department of Pathology and Laboratory Medicine, The University of Texas Medical School at Houston, University of Texas Health Science Center at Houston, Houston, Texas, USA.

PDGFR is an important target for novel anticancer therapeutics because it is overexpressed in a wide variety of malignancies. Recently, however, several anticancer drugs that inhibit PDGFR signaling have been associated with clinical heart failure. Understanding this effect of PDGFR inhibitors has been difficult because the role of PDGFR signaling in the heart remains largely unexplored. As described herein, we have found that PDGFR-β expression and activation increase dramatically in the hearts of mice exposed to load-induced cardiac stress. In mice in which *Pdgfrb* was knocked out in the heart in development or in adulthood, exposure to load-induced stress resulted in cardiac dysfunction and heart failure. Mechanistically, we showed that cardiomyocyte PDGFR-β signaling plays a vital role in stress-induced cardiac angiogenesis. Specifically, we demonstrated that cardiomyocyte PDGFR-β was an essential upstream regulator of the stress-induced paracrine angiogenic capacity (the angiogenic potential) of cardiomyocytes. These results demonstrate that cardiomyocyte PDGFR-β is a regulator of the compensatory cardiac response to pressure overload–induced stress. Furthermore, our findings may provide insights into the mechanism of cardiotoxicity due to anticancer PDGFR inhibitors.

Introduction

PDGF receptors and/or ligands are overexpressed in a wide variety of malignancies (1–4). In the past decade, a number of inhibitors of receptor tyrosine kinases (RTKs) whose targets include PDGFR have emerged as agents with remarkable efficacy in the treatment of human cancers (5–7). However, several of these agents have been linked to the development of cardiomyopathy in subsets of treated patients.

Recent reports indicate that the anticancer agent sunitinib, whose targets include PDGFR, causes cardiac dysfunction in up to 19% of treated patients (8), and we and others have reported the development of clinical heart failure in subsets of sunitinib-treated patients (8–10). Sorafenib, another RTK inhibitor that targets PDGFR, was recently associated with myocardial damage and cardiac dysfunction in renal cell carcinoma patients (10). In addition, imatinib, whose targets include PDGFR in addition to Abl kinase, has been linked to the development of cardiomyopathy (11), although this appears to be an infrequent clinical occurrence (12). Importantly, both sunitinib and sorafenib lead to the development of subacute, severe hypertension in substantial numbers of patients (8, 13), while imatinib rarely causes hypertension.

Linking the incidence of cardiomyopathy associated with anticancer PDGFR inhibitors with the relative incidences of hypertension associated with these drugs led us to hypothesize that PDGFR signaling in the heart may play a key role in the cardiac response to vascular stress such as hypertension. However, little is known regarding the role of PDGFR signaling in adult cardiomyocytes. We show here that cardiomyocyte PDGFR-β expression and activation rise dramatically in response to pressure overload–induced stress. Furthermore, we show that knockout of PDGFR-β in the cardiomyocyte results in cardiac dysfunction, heart failure, and a marked defect in stress-induced cardiac angiogenesis. Mechanistically, we demonstrate that PDGFR-β is an essential regulator of the paracrine angiogenic capacity, or angiogenic potential, of cardiomyocytes.

Results

PDGFR-β expression in cardiomyocytes increases dramatically in response to pressure overload–induced stress. We exposed C57BL/6 mice to transverse aortic constriction (TAC), in which a ligature is placed at the aortic arch, resulting in acute pressure overload. As expected, we observed profound increases in cardiac weight (Figure 1A) and cardiac thickness (Figure 1B) in mice exposed to TAC. Cardiac lysates from mice exposed to TAC exhibited increased levels of PDGFR-β persisting to 14 days after TAC (Figure 1C). Quantitative densitometry revealed a 10-fold increase in PDGFR-β protein levels in the heart 7 days after TAC (Figure 1D). Enhanced PDGFR-β expression after TAC was predominantly seen on cardiomyocytes (Figure 1E), as opposed to non-myocyte cells within the heart such as fibroblasts or endothelial cells. A substantial increase in phosphorylated, activated PDGFR-β was seen in the heart 7 days after TAC (Figure 1F) and 14 days after TAC (data not shown), suggesting that changes in PDGFR-β in the cardiomyocyte after TAC were functionally important. Marked increases in levels of phosphorylated Akt and ERK1/2, established down-

Conflict of interest: The authors have declared that no conflict of interest exists.
Citation for this article: *J Clin Invest.* 2010;120(2):472–484. doi:10.1172/JCI39434.

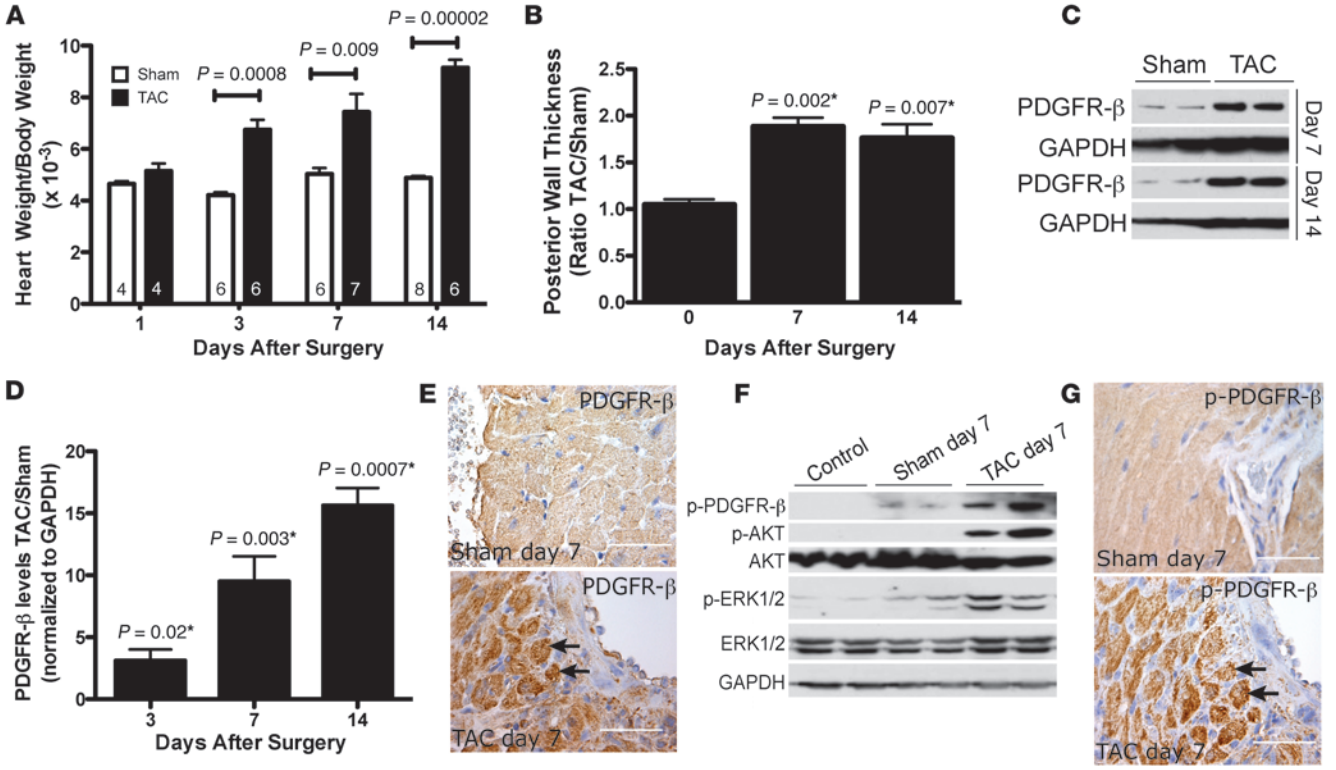

Figure 1

PDGFR-β expression and phosphorylation in cardiomyocytes increase dramatically in response to pressure overload stress. (**A**) Heart weight/body weight ratios in 8- to 12-week-old C57BL/6 mice exposed to TAC or sham surgery (Sham). (**B**) Ratio of the posterior wall thickness of hearts from mice exposed to TAC versus sham surgery. Day 0 indicates baseline levels, prior to surgery. (**C**) Western blot of PDGFR-β levels in cardiac lysates harvested after the indicated number of days from animals exposed to TAC or sham surgery. (**D**) Ratio of PDGFR-β levels (normalized for GAPDH) from cardiac lysates from animals exposed to TAC versus sham surgery at the indicated time points ($n = 4$ samples in each group). (**E**) Immunohistochemical staining for PDGFR-β in cardiac sections from mice exposed to sham surgery (upper panel) or TAC for 7 days. Arrows indicate cardiomyocytes intensely stained for PDGFR-β. Results are representative of at least 3 separate, independent cardiac samples. Scale bars: 50 μm. (**F**) Western blot probed for phospho-/total levels of PDGFR-β, Akt, and ERK1/2 in hearts of unoperated mice (Control) or mice 7 days after TAC or sham surgery. Results are representative of 4 samples in each group. (**G**) Immunohistochemical staining for phospho–PDGFR-β in cardiac sections from mice exposed to sham surgery (upper panel) or TAC for 7 days. Arrows indicate cardiomyocytes intensely stained for phospho–PDGFR-β. Scale bars: 50 μm. Asterisks indicate that statistical comparison was between TAC and sham surgery at the specified time point. *P* values were determined by unpaired, 2-tailed Student's *t* test.

stream effectors of PDGFR-β, were also observed in the heart after TAC. Immunohistochemistry with a phospho-specific PDGFR-β antibody demonstrated that phospho–PDGFR-β after TAC was increased predominantly in cardiomyocytes (Figure 1G). Levels of PDGFR-α were increased in the hearts of mice exposed to TAC compared with sham-operated mice (Supplemental Figure 1; supplemental material available online with this article; doi:10.1172/JCI39434DS1), but we observed no increase in phosphorylation of PDGFR-α (data not shown), suggesting a dominant biological role of PDGFR-β compared with PDGFR-α in the heart after exposure to load stress. We also observed significantly increased levels of local expression of the PDGFR-β ligands PDGF-B and PDGF-C 3 days after TAC (Supplemental Figure 2), while levels of PDGF-A and PDGF-D were significantly decreased in the heart 3 days after TAC, suggesting that dynamic changes in local PDGF expression may contribute to activation of PDGFR-β after TAC.

Cardiomyocyte PDGFR-β is not required for normal cardiac development or basal adult cardiac function. To further explore the role of PDGFR-β signaling in cardiac function, we constructed mice in which PDGFR-β was knocked out in cardiomyocytes. This was done by crossing mice expressing the Cre recombinase driven by the *Nkx2.5* promoter (*Nkx2.5-Cre* mice) (14) with mice in which PDGFR-β was flanked by loxP sites (*Pdgfrb*$^{fl/fl}$ mice) (15). Nkx2.5 is a cardiac-specific transcription factor that exhibits expression at high levels in the heart beginning at 9.5 dpc (14). *Nkx2.5-Cre:Pdgfrb*$^{fl/fl}$ mice (cardiac-specific PDGFR-β–knockout mice; *Pdgfrb*$^{Nkx\text{-}Cre}$) were born at the expected Mendelian frequency (data not shown) and were able to support pregnancy. To confirm that the knockout strategy was successful and specific, we isolated genomic DNA from the hearts of newborn *Pdgfrb*$^{Nkx\text{-}Cre}$ mice. The presence of the lower PCR band represents the Cre-excised allele (Figure 2A), and this was seen in the heart, but not in mouse tails or skeletal muscle, while the higher band, the nonexcised floxed allele, was markedly diminished in the heart compared with other tissues. Furthermore, representative Western blots from hearts of 4-week-old mice demonstrated reduced levels of PDGFR-β protein in *Pdgfrb*$^{Nkx\text{-}Cre}$ compared with *Pdgfrb*$^{fl/fl}$ controls (Figure 2B). Analysis of mutant embryos at 15.5 dpc revealed normal cardiac trabeculation and no evidence of septal or outflow tract abnormalities (data not shown), as observed in conventional knockout models of PDGF-B (16) and PDGFR-α (17).

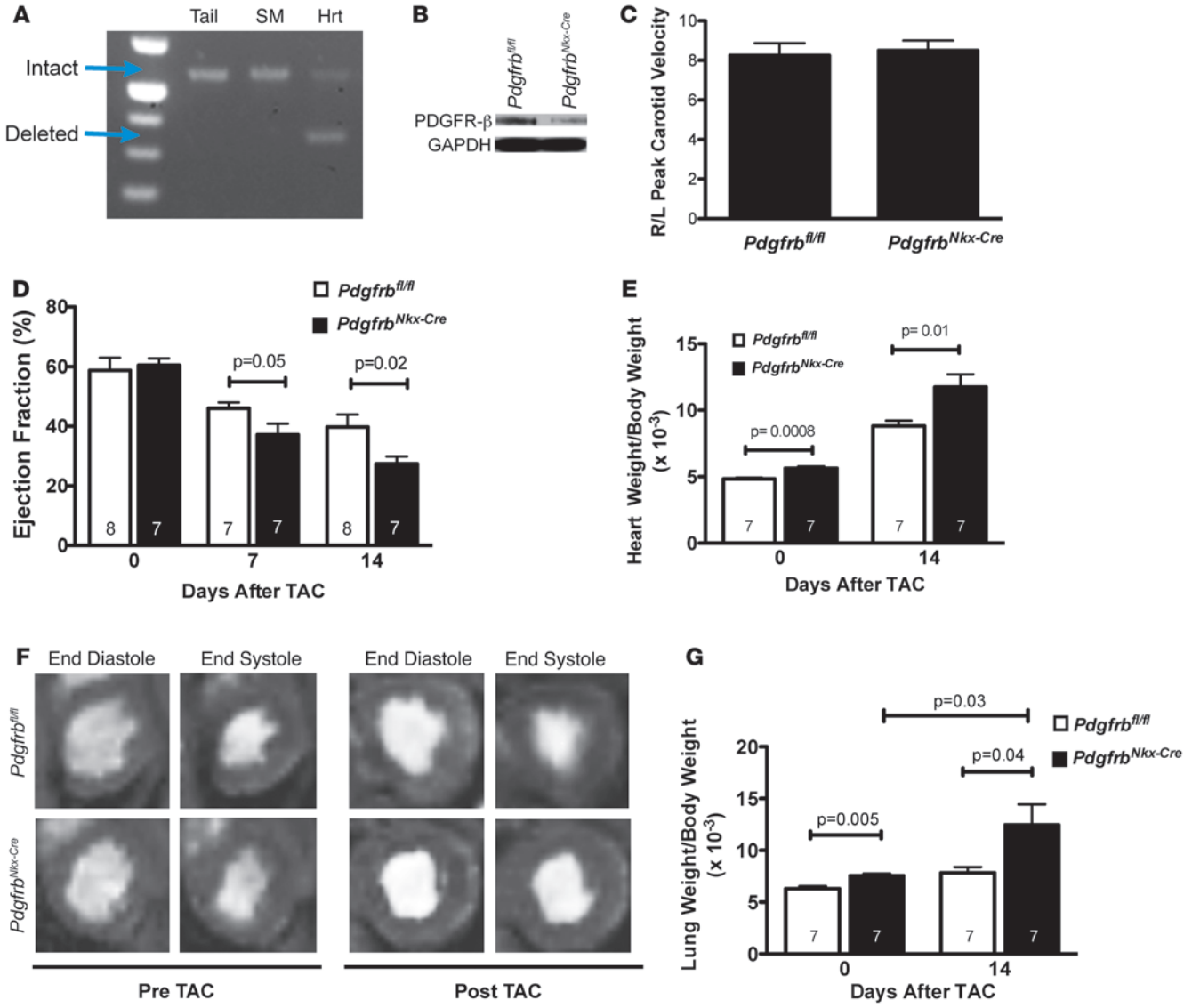

Figure 2

Cardiac-specific PDGFR-β–knockout mice develop ventricular dilatation and heart failure in response to pressure overload. (**A**) PCR of genomic DNA from tails, skeletal muscle (SM), or hearts (Hrt) from newborn cardiac-specific PDGFR-β–knockout mice ($Pdgfrb^{Nkx\text{-}Cre}$) mice using primer pairs specific for floxed allele (upper band) or deleted allele (lower band). Results are representative of 3 independent experiments. (**B**) Western blot of cardiac lysates from 4-week-old *Nkx2.5-Cre:*$Pdgfrb^{fl/fl}$ mice ($Pdgfrb^{Nkx\text{-}Cre}$) or non–Cre-expressing littermate control ($Pdgfrb^{fl/fl}$) mice probed with an antibody against PDGFR-β. (**C**) Ratio of right/left (R/L) peak carotid velocity 24 hours after 8- to 12-week-old $Pdgfrb^{Nkx\text{-}Cre}$ or $Pdgfrb^{fl/fl}$ mice were exposed to TAC (n = 8 in each group). (**D**) Cardiac ejection fraction of $Pdgfrb^{fl/fl}$ mice or $Pdgfrb^{Nkx\text{-}Cre}$ mice prior to TAC (day 0) or at various time points after TAC, as measured by MRI. (**E**) Heart weight/body weight ratios of $Pdgfrb^{fl/fl}$ versus $Pdgfrb^{Nkx\text{-}Cre}$ mice prior to TAC (day 0) or 14 days after TAC. (**F**) Representative short-axis MRI still frame images taken at the mid-ventricular level in $Pdgfrb^{fl/fl}$ or $Pdgfrb^{Nkx\text{-}Cre}$ mice prior to TAC exposure (left panels) or 14 days after TAC exposure (right panels). (**G**) Ratio of lung weight/body weight of $Pdgfrb^{fl/fl}$ versus $Pdgfrb^{Nkx\text{-}Cre}$ mice prior to TAC or 14 days after TAC. *P* values were determined by unpaired, 2-tailed Student's *t* test. Numbers inside the bars indicate the number of animals analyzed.

When animals were 6 weeks of age, we observed no significant difference in cardiac ejection fraction in $Pdgfrb^{Nkx\text{-}Cre}$ compared with $Pdgfrb^{fl/fl}$ or *Nkx2.5-Cre* control mice (Table 1). Notably, we did observe a small but significant increase in heart weight/body weight ratio in $Pdgfrb^{Nkx\text{-}Cre}$ compared with $Pdgfrb^{fl/fl}$ or *Nkx2.5-Cre* control mice, driven largely by nonsignificant increases in the thickness of the intraventricular septum and posterior walls. In addition, we observed small, significant increases in lung weight/body weight ratios in $Pdgfrb^{Nkx\text{-}Cre}$ mice. Importantly, cardiac ejection fractions, heart weights, and ventricular chamber sizes were normal in 8-month-old $Pdgfrb^{Nkx\text{-}Cre}$ mice and were not different from those of $Pdgfrb^{fl/fl}$ or *Nkx2.5-Cre* controls (data not shown). Thus, cardiomyocyte PDGFR-β signaling does not appear to play a key role in cardiac development or in basal adult cardiac function.

PDGFR-β cardiac-specific knockout mice develop ventricular dilatation and heart failure in response to pressure overload. To determine

Table 1
Cardiac function and morphometry of 6-week-old cardiac-specific PDGFR-β–knockout mice (*Pdgfrb*$^{Nkx\text{-}Cre}$) compared with controls (*Nkx2.5-Cre* and *Pdgfrb*$^{fl/fl}$)

	Nkx2.5-Cre	*Pdgfrb*$^{fl/fl}$	*Pdgfrb*$^{Nkx\text{-}Cre}$	ANOVA *P* value
BW (g)	21.7 ± 1.6	23.1 ± 1.1	20.9 ± 1.2	0.43
HW (mg)	111.4 ± 11.5	112.6 ± 4.7	118.2 ± 8.5	0.84
HW/BW (mg/g)	5.06 ± 0.19	4.83 ± 0.10	5.62 ± 0.15	0.004
LW (mg)	142.1 ± 13.8	146.0 ± 6.0	158.7 ± 12.9	0.57
LW/BW (mg/g)	6.47 ± 0.20	6.29 ± 0.25	7.53 ± 0.22	0.002
EF (%)	57.7 ± 2.1	58.8 ± 4.3	60.5 ± 2.3	0.81
PWTd (mm)	0.86 ± 0.04	0.92 ± 0.07	1.08 ± 0.09	0.08
IVSTd (mm)	0.68 ± 0.06	0.71 ± 0.05	0.85 ± 0.08	0.46

BW, body weight; HW, heart weight; LW, lung weight; EF, ejection fraction; PWTd, posterior wall thickness in diastole; IVSTd, intraventricular septal thickness in diastole. n = 8 animals assessed in control groups and n = 7 animals in *Pdgfrb*$^{Nkx\text{-}Cre}$ group. P values were determined by ANOVA, and significant differences between mutant and control groups were confirmed by Tukey's test.

whether cardiomyocyte PDGFR-β is a required component of the cardiac response to pressure overload, we exposed 8- to 12-week-old *Pdgfrb*$^{Nkx\text{-}Cre}$ mice or littermate *Pdgfrb*$^{fl/fl}$ controls to TAC stress. The ratio of right-to-left carotid flow velocities, a surrogate of the degree of aortic impedance imposed in our TAC model (18), was similar in *Pdgfrb*$^{Nkx\text{-}Cre}$ mice and *Pdgfrb*$^{fl/fl}$ controls (Figure 2C). Notably, cardiac ejection fractions in *Pdgfrb*$^{Nkx\text{-}Cre}$ mice were significantly decreased compared with those in *Pdgfrb*$^{fl/fl}$ controls at 7 days after TAC, with a further decline 14 days after TAC (Figure 2D). In addition, *Pdgfrb*$^{Nkx\text{-}Cre}$ mice displayed increased heart weight/body weight ratios 14 days after TAC (Figure 2E), indicative of enhanced pathologic hypertrophy in *Pdgfrb*$^{Nkx\text{-}Cre}$ mice after TAC stress. Cardiomyocyte cross-sectional area 14 days after TAC was significantly increased in *Pdgfrb*$^{Nkx\text{-}Cre}$ mice compared with *Pdgfrb*$^{fl/fl}$ controls (Supplemental Figure 3), further indicative of a pathologic hypertrophy phenotype. Representative short-axis systolic and diastolic still frame MRI images (Figure 2F) demonstrated the acquired cardiac dysfunction seen in *Pdgfrb*$^{Nkx\text{-}Cre}$ mice 14 days after TAC. Lung weights were significantly increased in *Pdgfrb*$^{Nkx\text{-}Cre}$ mice 14 days after TAC (Figure 2G), indicative of pulmonary edema and functional heart failure.

Inducible, cardiac-specific PDGFR-β–knockout mice develop severe heart failure in response to TAC stress. Our findings in *Pdgfrb*$^{Nkx\text{-}Cre}$ mice suggest that PDGFR-β signaling plays a key role in the cardiac response to load stress. However, we could not exclude the possibility that developmental abnormalities and/or expression of Cre recombinase in *Pdgfrb*$^{Nkx\text{-}Cre}$ mice predispose these mice to cardiac failure upon exposure to TAC. To specifically determine the role of PDGFR-β signaling in the adult cardiac response to load-induced stress, we crossed *Pdgfrb*$^{fl/fl}$ mice with mice expressing the *MerCreMer* transgene driven by the α-MHC promoter (*MerCreMer* mice), which exhibit high cardiac levels of nuclear Cre recombinase activity only in the presence of tamoxifen (19). Hearts from α-*MHC-MerCreMer: Pdgfrb*$^{fl/fl}$ mice (inducible, cardiac-specific PDGFR-β–knockout mice, *Pdgfrb*^{MerCre}) expressed reduced levels of PDGFR-β (Figure 3A) compared with non–Cre-expressing, tamoxifen-treated *Pdgfrb*$^{fl/fl}$ controls. We observed no compensatory differences in the expression of PDGFR-α in the hearts of *Pdgfrb*^{MerCre} mice compared with *Pdgfrb*$^{fl/fl}$ control mice (Supplemental Figure 4). Inducible mutants were exposed to a similar degree of TAC stress as either *Pdgfrb*$^{fl/fl}$ or *MerCreMer* control mice (Figure 3B). Heart weights of tamoxifen-treated *Pdgfrb*^{MerCre} mice significantly increased in response to TAC compared with those of tamoxifen-treated *Pdgfrb*$^{fl/fl}$ or *MerCreMer* controls (Figure 3C). Cardiomyocyte cross-sectional area 14 days after TAC was significantly increased in *Pdgfrb*^{MerCre} mice compared with *Pdgfrb*$^{fl/fl}$ and *MerCreMer* controls (Supplemental Figure 5), further indicative of a pathologic hypertrophy phenotype in *Pdgfrb*^{MerCre} mice. *Pdgfrb*^{MerCre} mice experienced significant declines in cardiac ejection fraction 7 days after TAC and severe cardiac dysfunction 14 days after TAC compared with *Pdgfrb*$^{fl/fl}$ or *MerCreMer* controls (Figure 3D). Cardiac dysfunction and pathologic hypertrophy in *Pdgfrb*^{MerCre} mice was associated with increased ventricular dilatation, seen 14 days after TAC in *Pdgfrb*^{MerCre} mice (Figure 3E). Representative hearts from *Pdgfrb*^{MerCre} mice and *Pdgfrb*$^{fl/fl}$ controls 14 days after TAC demonstrate the observed cardiac dilatation (Figure 3F). MRI cine videos demonstrate the load-induced dilated cardiomyopathy phenotype in *Pdgfrb*^{MerCre} mice (Supplemental Video 1). Significant increases in lung weight, indicative of pulmonary edema, were seen in *Pdgfrb*^{MerCre} mice compared with either *MerCreMer* or *Pdgfrb*$^{fl/fl}$ control mice beginning at 7 days after TAC, and differences were even more striking 14 days after TAC (Figure 3G). Expression of B-type natriuretic peptide (BNP), a marker of pathologic hypertrophy and heart failure (20), was increased in hearts of *Pdgfrb*^{MerCre} mice as early as 3 days after exposure to TAC (Figure 3H).

Inducible cardiac-specific PDGFR-β–knockout mice exhibit impaired activation of Akt and MAPK pathways in the progression to heart failure. To gain insight into the mechanism of load-induced heart failure in *Pdgfrb*^{MerCre} mice, we measured changes in the PI3K and MAPK pathways, effectors of PDGFR signaling (21) known to mediate the compensatory cardiac response to load-induced stress (22). Levels of phosphorylation of p38 kinase, whose role in cardiac protection is ambiguous (23), were significantly decreased in hearts of *Pdgfrb*^{MerCre} mice at 7 and 14 days after TAC (Figure 4, A and B). Phosphorylation of ERK1/2, previously demonstrated to protect the heart in response to load stress (24), was significantly decreased at 14 but not 7 days after TAC in *Pdgfrb*^{MerCre} mice (Figure 4, A and C). A similar pattern was observed with respect to phosphorylation of JNK kinase (Figure 4A). In addition, levels of phosphorylation of the protein kinase Akt were significantly reduced in *Pdgfrb*^{MerCre} mice compared with *Pdgfrb*$^{fl/fl}$ controls 14 days after exposure to TAC (Figure 4, D and E).

We also observed diminished phosphorylation of both Akt and ERK1/2 in the hearts of *Pdgfrb*$^{Nkx\text{-}Cre}$ mice compared with controls 14 days after TAC stress (Supplemental Figure 6). Since both Akt and ERK1/2 exert cardioprotective effects in part via inhibition of apoptosis, we sought to determine whether cardiomyocyte apoptosis after TAC was different in *Pdgfrb*^{MerCre} mice compared with *Pdgfrb*$^{fl/fl}$ controls. Consistent with our biochemical findings, the number of apoptotic cardiomyocytes was increased in *Pdgfrb*^{MerCre} mice 7 days after TAC and continued to rise 14 days after TAC (Figure 4F). Overall, these findings suggest that PDGFR-β signaling in the heart may participate in modulating the activation of cardioprotective protein kinases in the progression of heart failure due to pressure overload.

Angiogenic gene expression profile correlates with defective microvascular function in inducible, cardiac-specific PDGFR-β–knockout mice upon expo-

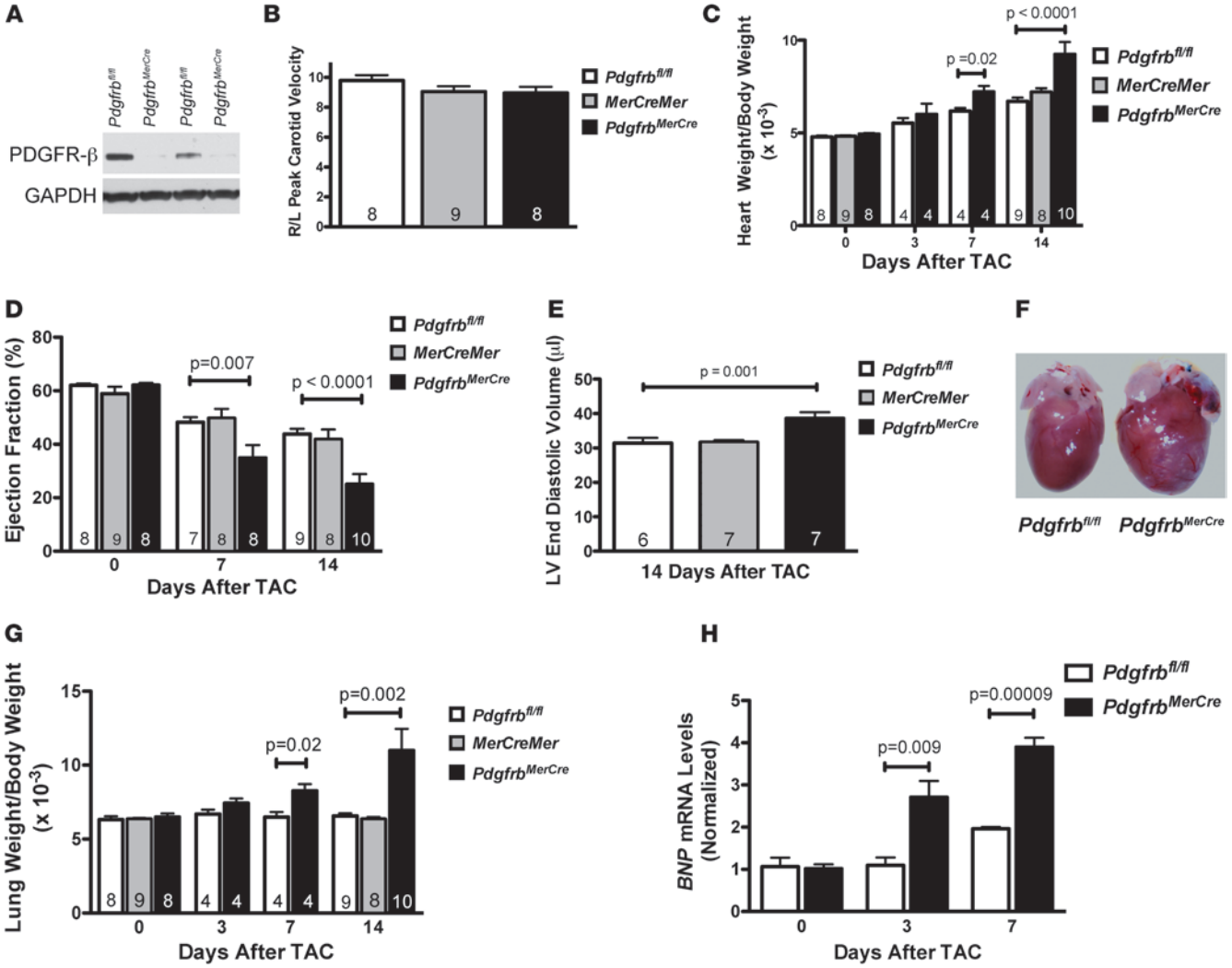

Figure 3

Inducible, cardiac-specific PDGFR-β–knockout mice develop severe heart failure in response to pressure overload. (**A**) Expression of PDGFR-β in hearts from α-*MHC-MerCreMer:Pdgfrb*$^{fl/fl}$ mice (inducible, cardiac-specific PDGFR-β–knockout mice, *Pdgfrb*^{MerCre}) or *Pdgfrb*$^{fl/fl}$ controls harvested 7 days after exposure to tamoxifen. Results are representative of 4 independent hearts assessed from each group. (**B**) Ratio of right/left peak carotid velocity 24 hours after 8- to 12-week-old *Pdgfrb*^{MerCre}, *MerCreMer*, or *Pdgfrb*$^{fl/fl}$ mice were exposed to TAC. All groups of mice were treated with tamoxifen in an identical manner prior to baseline analysis and exposure to TAC stress (see Methods). (**C**) Heart weight/body weight ratios in 8- to 12-week-old *Pdgfrb*^{MerCre}, *MerCreMer*, or *Pdgfrb*$^{fl/fl}$ mice after TAC. (**D**) Cardiac ejection fraction of *Pdgfrb*^{MerCre}, *MerCreMer*, or *Pdgfrb*$^{fl/fl}$ mice prior to TAC or at time points after TAC, as measured by MRI. (**E**) LV end diastolic volume of *Pdgfrb*^{MerCre}, *MerCreMer*, or *Pdgfrb*$^{fl/fl}$ mice 14 days after TAC. (**F**) Representative hearts from *Pdgfrb*$^{fl/fl}$ or *Pdgfrb*^{MerCre} mice 14 days after TAC. (**G**) Expression levels of BNP assessed from mRNA from hearts of *Pdgfrb*$^{fl/fl}$ or *Pdgfrb*^{MerCre} mice prior to TAC or at time points after TAC (n = 4 samples per group at each time point). (**H**) Ratio of lung weight/body weight of *Pdgfrb*^{MerCre}, *MerCreMer*, or *Pdgfrb*$^{fl/fl}$ mice at baseline or at time points after TAC. *P* values were determined by ANOVA, and significant differences between *Pdgfrb*^{MerCre} and control (*MerCreMer* and *Pdgfrb*$^{fl/fl}$) mice were confirmed with Tukey's test. Numbers inside the bars indicate the number of animals analyzed.

sure to load stress. The majority of the biochemical changes described in Figure 4 occurred after the initiation of the heart failure phenotype in *Pdgfrb*^{MerCre} mice upon exposure to pressure overload. To understand the initiating biological mechanism of heart failure in *Pdgfrb*^{MerCre} mice, we focused on identifying biologic changes between *Pdgfrb*^{MerCre} mice and *Pdgfrb*$^{fl/fl}$ controls at time points preceding the development of overt heart failure using a broad approach, namely microarray gene expression studies. Of the genes that were differentially expressed (Supplemental Table 1), we focused on a group of genes that exhibited the pattern depicted in Figure 5A — genes expressed in the heart at similar levels in *Pdgfrb*^{MerCre} mice and *Pdgfrb*$^{fl/fl}$ controls prior to TAC but increased in *Pdgfrb*$^{fl/fl}$ controls compared with *Pdgfrb*^{MerCre} mice at early time points (3 and 7 days) after TAC. Functional annotation clustering of this subset of genes revealed an enrichment of genes that participate in multiple facets of angiogenesis (Figure 5B), including endothelial cell proliferation (e.g., *Agtrl1*; ref. 25), endothelial cell migration (*Angpt1*; ref. 26), extracellular matrix remodeling (e.g., *Mmp2*; ref. 27), and proangiogenic transcription factors (e.g., *Elk3*). We thus postulated that PDGFR-β signaling in the cardiomyocyte

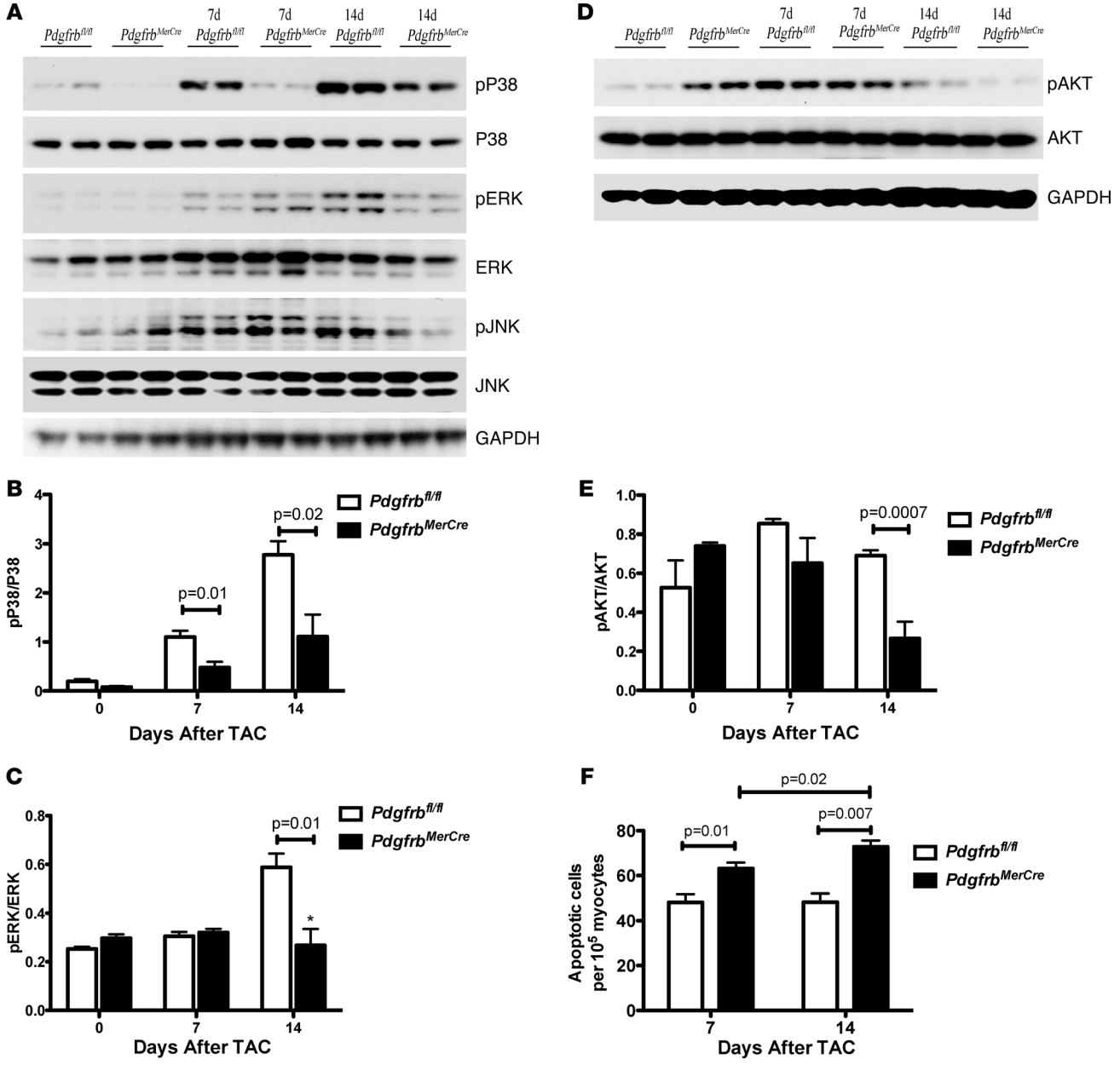

Figure 4

Inducible, cardiac-specific PDGFR-β–knockout mice exhibit impaired activation of Akt and MAPK pathways in the progression to heart failure. Representative Western blots from cardiac lysates of *Pdgfrb*^{MerCre} mice (inducible, cardiac-specific PDGFR-β–knockout mice) or *Pdgfrb*$^{fl/fl}$ controls harvested prior to TAC or at indicated time points after TAC probed for (**A**) phospho-/total p38, phospho-/total ERK1/2, and phospho/total JNK or (**D**) phospho-/total Akt. (**B**, **C**, and **E**) Quantification by densitometry (n = 4 independent samples per group per time point) of ratios of (**B**) phospho-/total p38, (**C**) phospho-/total ERK1/2, or (**E**) phospho-/total Akt. (**F**) Number of apoptotic cells per 100,000 myocytes from hearts of *Pdgfrb*^{MerCre} mice or *Pdgfrb*$^{fl/fl}$ controls assessed at 7 or 14 days after TAC. Data represent results from 2 spatially separated samples from 3 separate animals from each group at each time point. *P* values were determined by unpaired, 2-tailed Student's *t* test.

regulates cardiac angiogenesis in response to stress. This hypothesis correlates with reports indicating that the cardiomyocyte itself is a paracrine cell functioning to enhance blood vessel growth during conditions of increased substrate demand (28–30).

To test this hypothesis, we measured coronary flow reserve (CFR), which provides a robust assessment of coronary microvascular function in mice (31) and humans (32). Representative tracings (Figure 5C) of coronary flow in response to vasodilator stimulus (2.5% inhaled isoflurane; ref. 33) demonstrate reduced hyperemic coronary flow in *Pdgfrb*^{MerCre} mice at baseline and after TAC. Quantification of CFR demonstrated a significant reduction at baseline in *Pdgfrb*^{MerCre} mice compared with either *MerCreMer* or *Pdgfrb*$^{fl/fl}$ controls (Figure 5D). By 7 days after TAC, *Pdgfrb*^{MerCre} mice had minimal augmentation of coronary flow in response to

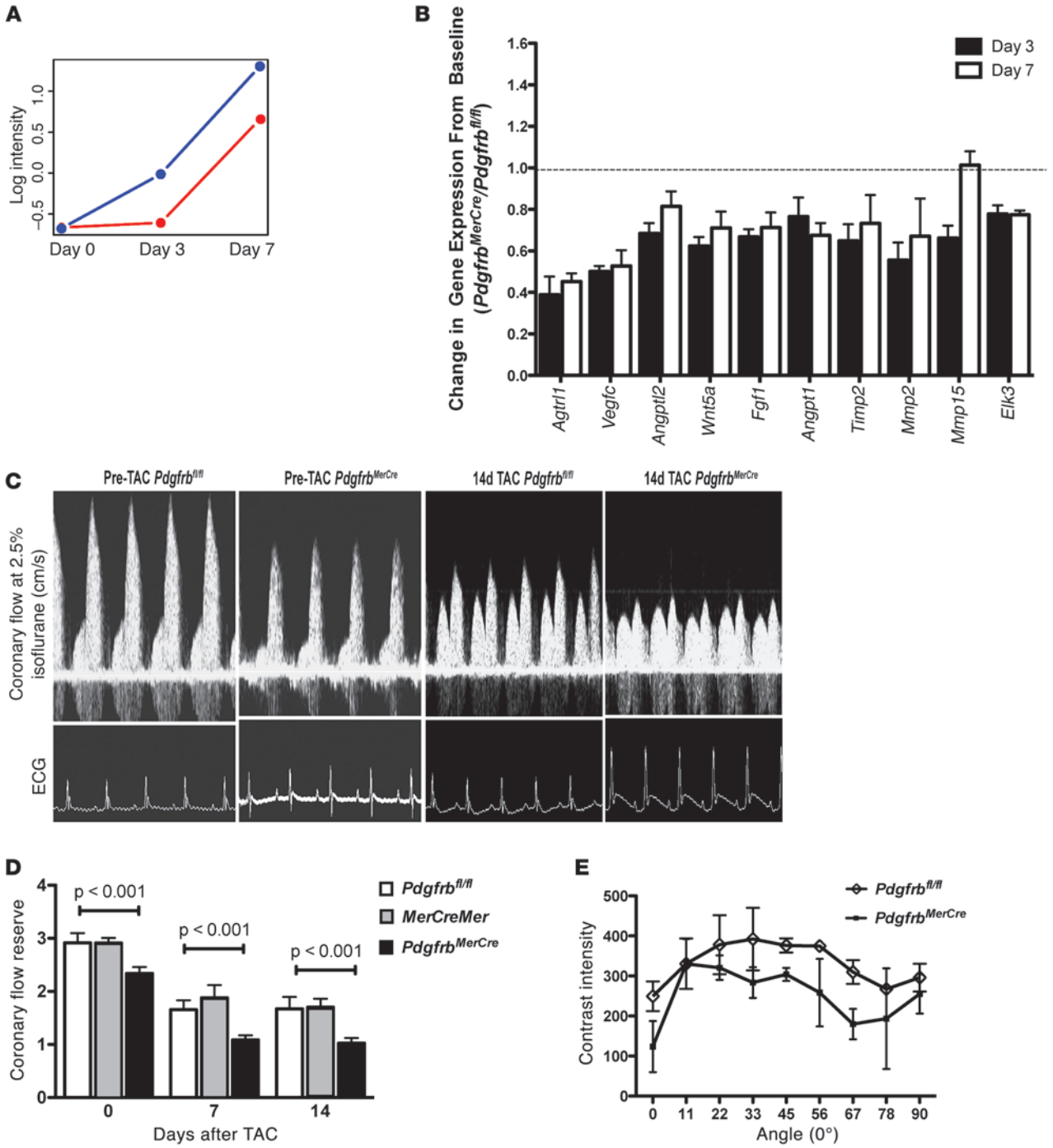

Figure 5

Angiogenic gene expression profile correlates with defective microvascular function in inducible, cardiac-specific PDGFR-β–knockout mice upon exposure to load stress. (**A**) Pattern of change of genes of interest over time prior to and after TAC (red, $Pdgfrb^{MerCre}$; blue, $Pdgfrb^{fl/fl}$). (**B**) Change of expression from baseline (ratio of $Pdgfrb^{MerCre}$ to $Pdgfrb^{fl/fl}$) of genes associated with multiple aspects of angiogenesis ($n = 4$ samples in each group at each time point). (**C**) Representative ultrasound tracings of maximal coronary flow after hyperemic stimulus prior to TAC or 14 days after TAC in control $Pdgfrb^{fl/fl}$ or $Pdgfrb^{MerCre}$ mice. (**D**) Quantification of CFR in $Pdgfrb^{fl/fl}$, *MerCreMer*, or $Pdgfrb^{MerCre}$ mice ($n = 7$ in each group at each time point). (**E**) Quantification of cardiac perfusion as assessed by myocardial contrast uptake (see Methods) from 0° (anterior wall of the left ventricle) to 90° (lateral wall of left ventricle) 14 days after TAC in $Pdgfrb^{MerCre}$ or $Pdgfrb^{fl/fl}$ control mice ($n = 3$ $Pdgfrb^{MerCre}$ mice, $n = 4$ $Pdgfrb^{fl/fl}$ control mice). *P* values were determined by ANOVA, and significant differences between $Pdgfrb^{MerCre}$ and control ($Pdgfrb^{fl/fl}$ and *MerCreMer)* mice were confirmed with Tukey's test.

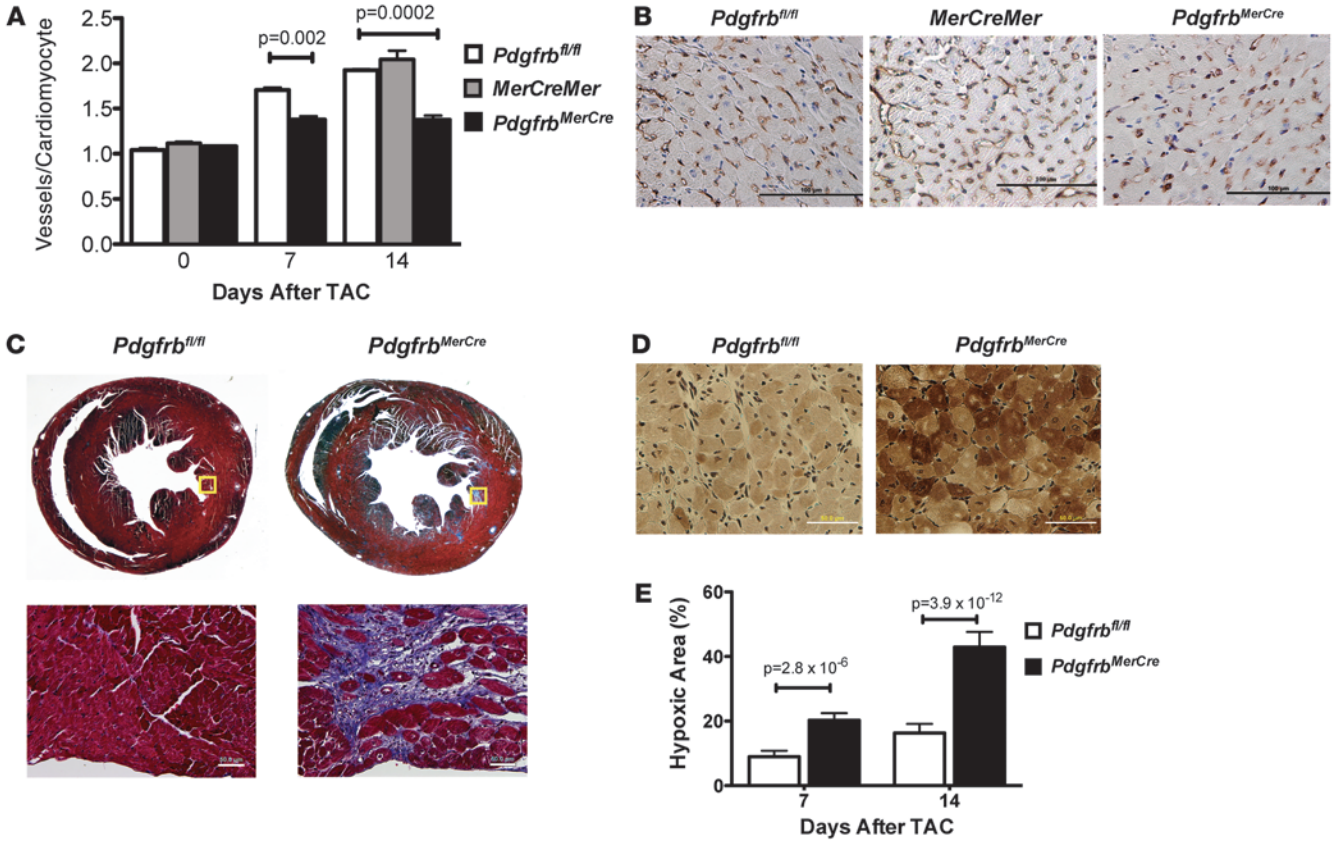

Figure 6
Impaired angiogenesis and evidence of ischemic injury in the hearts of inducible, cardiac-specific PDGFR-β–knockout mice upon exposure to load stress. (**A**) Microvessel number per cardiomyocyte in *Pdgfrb*$^{fl/fl}$, *MerCreMer*, or *Pdgfrb*^{MerCre} mice at baseline (day 0) or at time points after TAC. (**B**) Representative photomicrographs of cardiac sections stained with an anti-CD31 antibody from *Pdgfrb*$^{fl/fl}$, *MerCreMer*, or *Pdgfrb*^{MerCre} hearts 14 days after TAC. Scale bars: 100 μm. (**C**) Low-power (original magnification, ×15) photomicrographs of representative Masson's trichrome–stained cardiac sections from *Pdgfrb*$^{fl/fl}$ or *Pdgfrb*^{MerCre} mice 14 days after TAC reveal diffuse, subendocardial fibrosis in hearts of *Pdgfrb*^{MerCre} exposed to load stress (upper panels). High-power photomicrographs of portion of sections in **C** indicated by boxed region (lower panels). Scale bars: 50 μm. (**D**) Representative photomicrographs of cardiac sections from *Pdgfrb*^{MerCre} or *Pdgfrb*$^{fl/fl}$ control mice assessed for hypoxia (see Methods) 14 days after TAC. Scale bars: 50 μm. (**E**) Quantification of hypoxic area in hearts of *Pdgfrb*^{MerCre} or *Pdgfrb*$^{fl/fl}$ control mice after TAC. Data represent mean of multiple fields from independent sections from 3 separate mice in each group at each time point.

vasodilator stimulus (CFR = 1), suggestive of a severe coronary microvascular defect. To determine whether *Pdgfrb*^{MerCre} mice had a global decline in myocardial perfusion in response to TAC, we used a microbubble perfusion method, producing a contrast-enhanced ultrasound signal in the myocardium that is directly proportional to perfusion (34). Using this technique throughout all assessable portions of the heart (the anterior and lateral segments of the left ventricle), we observed a reduction in myocardial perfusion in *Pdgfrb*^{MerCre} mice compared with *Pdgfrb*$^{fl/fl}$ controls (Figure 5E). Overall myocardial perfusion was reduced by 24.6% in inducible-mutant mice compared with controls 14 days after TAC (n = 3 *Pdgfrb*^{MerCre} mice, n = 4 *Pdgfrb*$^{fl/fl}$ mice, P = 0.01).

Impaired angiogenesis and evidence of ischemic injury in the hearts of inducible, cardiac-specific PDGFR-β–knockout mice upon exposure to load stress. Recent work demonstrates that angiogenesis is a crucial adaptive mechanism accompanying cardiac hypertrophy and manifesting as an increased number of coronary microvessels per cardiomyocyte (29). To determine whether coronary angiogenesis in response to pressure overload was impaired in *Pdgfrb*^{MerCre} mice, we quantified coronary microvessels at baseline or after TAC exposure. The number of CD31 microvessels per myocyte at baseline was not different in the hearts of *Pdgfrb*^{MerCre} mice compared with *Pdgfrb*$^{fl/fl}$ controls (Figure 6A). In contrast, while *Pdgfrb*$^{fl/fl}$ and *MerCreMer* control mice had a rise in coronary microvessels per cardiomyocyte in response to TAC consistent with previous findings (29), this increase was significantly blunted in *Pdgfrb*^{MerCre} mice at 7 and 14 days after TAC. Representative photomicrographs from hearts 14 days after TAC demonstrate the reduction in microvascular density in hearts of *Pdgfrb*^{MerCre} mice compared with *MerCreMer* or *Pdgfrb*$^{fl/fl}$ controls (Figure 6B).

Histologically, hearts from *Pdgfrb*^{MerCre} mice demonstrated a significant increase in fibrosis (Figure 6C) distributed throughout the subendocardium, the portion of the heart most susceptible to ischemic injury. To determine whether the reduction in angiogenesis resulted in functional myocardial ischemia, we used 2-nitroimidazole, an immunochemical marker for cardiac hypoxia (29). We observed a significant increase in myocardial hypoxia in *Pdgfrb*^{MerCre} mice 7 days after TAC (Figure 6E) and a more dra-

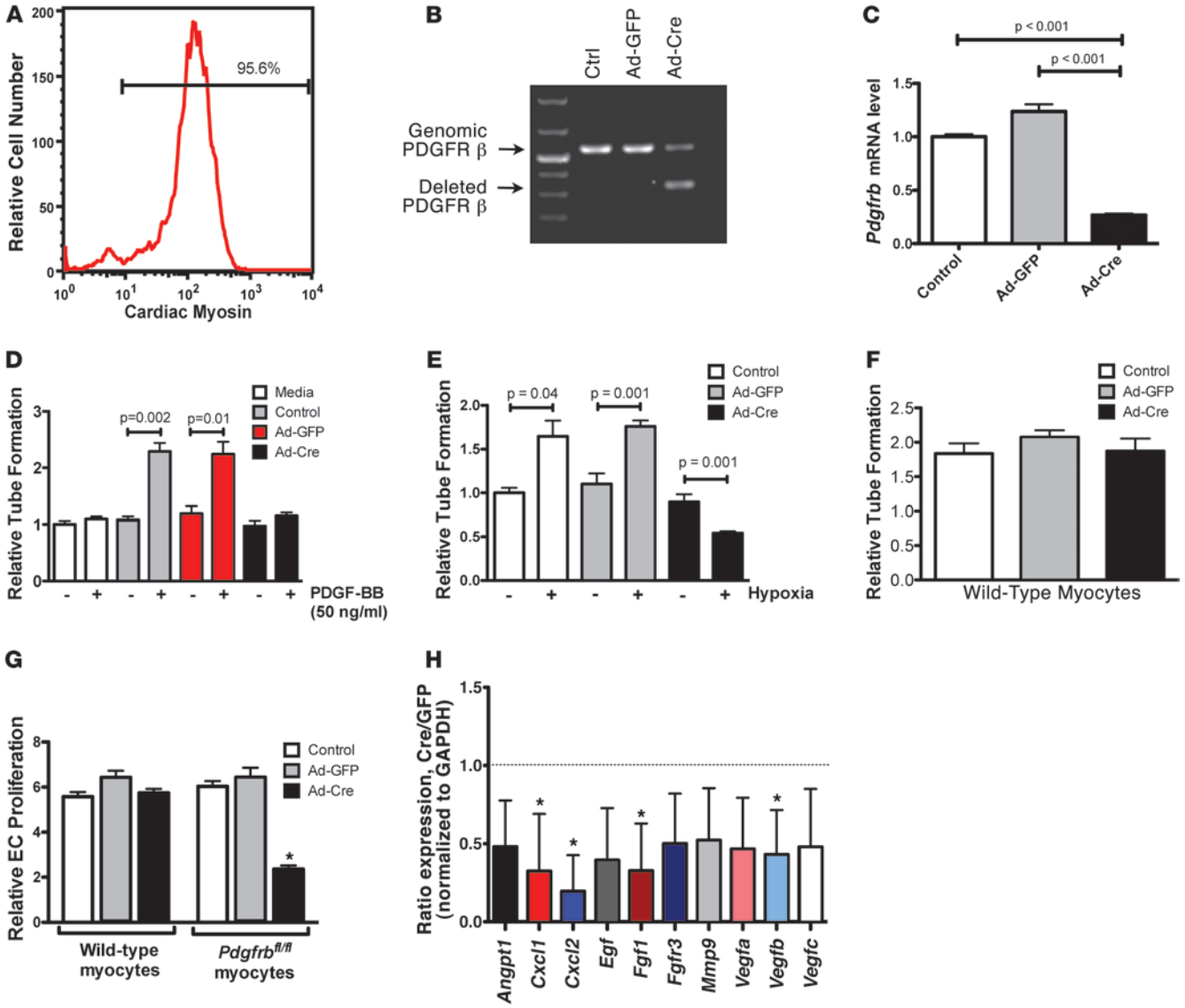

Figure 7

Cardiomyocyte PDGFR-β is an upstream regulator of the paracrine angiogenic capacity of cardiomyocytes. (**A**) FACS analysis of cardiomyocytes from *Pdgfrb*$^{fl/fl}$ mice stained with anti–sarcomeric myosin antibody. (**B**) Genomic PCR of cardiomyocytes from *Pdgfrb*$^{fl/fl}$ mice before infection (Ctrl) or after infection with Ad-GFP or Ad-Cre using primers for floxed allele (upper band) or deleted allele (lower band). (**C**) Quantitative RT-PCR for PDGFR-β expression (normalized to GAPDH) using RNA derived from cardiomyocytes from *Pdgfrb*$^{fl/fl}$ mice before infection (Control) or after infection with Ad-GFP or Ad-Cre. (**D**) Relative tube-forming capacity of conditioned media from cardiomyocytes from *Pdgfrb*$^{fl/fl}$ mice before infection (Control) or after infection with Ad-GFP or Ad-Cre with or without exogenous PDGF-BB. (**E**) Relative tube-forming capacity of conditioned media from cardiomyocytes from *Pdgfrb*$^{fl/fl}$ mice before infection or after infection with Ad-GFP or Ad-Cre under normoxic or hypoxic conditions. (**F**) Relative tube-forming capacity of conditioned media from cardiomyocytes from wild-type mice before or after infection with Ad-GFP or Ad-Cre and subsequent exposure to hypoxia. (**G**) Relative endothelial cell proliferation in conditioned media from wild-type and *Pdgfrb*$^{fl/fl}$ cardiomyocytes before or after infection with Ad-GFP or Ad-Cre and exposed to hypoxia. **P* < 0.001. (**H**) Ratio of reduction in expression (quantitative RT-PCR, normalized to GAPDH) of proangiogenic genes in cardiomyocytes from *Pdgfrb*$^{fl/fl}$ mice infected with Ad-Cre or Ad-GFP and exposed to hypoxia. **P* < 0.05. Data were derived from 4 independent experiments.

matic increase in hypoxia in the hearts of *Pdgfrb*^{MerCre} mice 14 days after TAC, visually demonstrated in Figure 6D. Biochemically, we observed increased levels of the transcription factor HIF-1α, whose expression increases in the ischemic heart (35), 7 days after TAC in *Pdgfrb*^{MerCre} mice compared with *Pdgfrb*$^{fl/fl}$ controls (Supplemental Figure 7), along with increased levels of the HIF-1α–dependent factor VEGF-A. However, 14 days after TAC, both HIF-1α and VEGF-A levels were significantly reduced in the hearts of *Pdgfrb*^{MerCre} mice despite profound tissue hypoxia. Taken together, our findings demonstrate that loss of cardiomyocyte PDGFR-β signaling results in a functional and structural defect in coronary microvascular flow accompanied by evidence of global myocardial ischemia in response to pressure overload–induced stress.

Cardiomyocyte PDGFR-β is an essential regulator of the paracrine angiogenic capacity of cardiomyocytes. Our in vivo observations demonstrate that loss of cardiomyocyte PDGFR-β results in load-induced

cardiac dysfunction associated with impairment in cardiac angiogenesis. Based upon our gene expression data (Figure 5, A and B), we hypothesized that PDGFR-β is a regulator of the paracrine angiogenic capacity, or angiogenic potential, of cardiomyocytes. To test this hypothesis, we isolated a highly purified population of neonatal cardiomyocytes from *Pdgfrb*$^{fl/fl}$ mice (Figure 7A). In vitro infection of these cardiomyocytes with Ad-Cre, but not with Ad-GFP, resulted in deletion of the floxed allele, detectable by PCR of genomic DNA (Figure 7B). Cre-mediated deletion of the floxed PDGFR-β allele from isolated cardiomyocytes resulted in a marked decrease in mRNA encoding PDGFR-β (Figure 7C).

Using this primary cardiomyocyte model, we first explored the ability of PDGF stimulation to enhance the ability of cardiomyocytes to support angiogenesis. In experiments in which cardiomyocytes from *Pdgfrb*$^{fl/fl}$ mice were used, conditioned media from control, noninfected cardiomyocytes, Ad-GFP–infected cardiomyocytes, or Ad-Cre cardiomyocytes was harvested before and after treatment with PDGF-BB or vehicle control. Conditioned media from control or Ad-GFP cardiomyocytes demonstrated a marked increase in the capacity to promote endothelial tube formation (a surrogate assay to assess the angiogenic capacity of cardiomyocytes) after treatment with PDGF-BB (Figure 7D), an effect not directly attributable to PDGF-BB (see Media, white bars). In contrast, the angiogenic capacity of conditioned media from cardiomyocytes in which PDGFR-β was deleted by Ad-Cre infection was not enhanced by PDGF-BB treatment. These findings demonstrate that PDGF-BB potently enhances the paracrine angiogenic capacity of cardiomyocytes in a PDGFR-β–dependent manner.

To determine whether PDGFR-β is a required component of the angiogenic potential of cardiomyocytes under conditions of physiologic stress, we exposed control, Ad-GFP–infected, or Ad-Cre–infected neonatal cardiomyocytes from *Pdgfrb*$^{fl/fl}$ mice to hypoxia, then harvested the conditioned media from these myocytes and tested its ability to support endothelial tube formation. Hypoxia significantly increased the capacity of conditioned media from control and Ad-GFP cardiomyocytes to support tube formation (Figure 7E). In contrast, we saw a reduction in the angiogenic capacity of conditioned media from Ad-Cre–infected, PDGFR-β–deleted cardiomyocytes upon exposure to hypoxic stress. To determine whether Ad-Cre infection had a direct toxic effect on the angiogenic capacity of cardiomyocytes, we infected control neonatal cardiomyocytes (not bearing the PDGFR-β floxed allele) with Ad-Cre or Ad-GFP and exposed these myocytes to hypoxia. As shown in Figure 7F, Ad-Cre infection had no effect on the paracrine ability of cardiomyocytes to support endothelial tube formation in response to hypoxia. As an independent measure of the PDGFR-β–dependent paracrine angiogenic capacity of cardiomyocytes, we found that conditioned media from Ad-Cre–infected cardiomyocytes from *Pdgfrb*$^{fl/fl}$ mice exposed to hypoxia had an impairment in the ability to support in vitro endothelial cell proliferation compared with Ad-GFP or control cardiomyocytes (Figure 7G). Experiments using wild-type cardiomyocytes demonstrated that this impairment in promoting endothelial cell proliferation is not attributable to Ad-Cre infection (Figure 7G). Furthermore, we identified a series of factors known to enhance in vivo angiogenesis that demonstrated a trend toward reduced expression in Ad-Cre–infected, PDGFR-β–deficient cardiomyocytes compared with control, Ad-GFP–infected cardiomyocytes after both cell models were exposed to hypoxia in vitro (Figure 7H), including statistically significant reductions in expression of *Cxcl1*, *Cxcl2,* and *Fgf1*. Thus, our findings demonstrate that PDGFR-β is an essential regulator of the angiogenic capacity of cardiomyocytes in response to hypoxic stress, in part through regulation of a program of expression of angiogenic factors. These findings are consistent with and provide a direct mechanistic basis for the cardiac dysfunction and impairment of load stress–induced angiogenesis observed in cardiac-specific PDGFR-β–knockout mice.

Discussion

We show here that PDGFR-β is an indispensable component of the cardiac response to pressure overload–induced stress. The robustness of our findings is reflected in the similarity of phenotype in 2 independent but overlapping knockout systems. Mechanistically, our findings suggest that PDGFR-β signaling is an important upstream regulator of the angiogenic potential of the cardiomyocyte in response to stress. The notion that PDGFR signaling regulates proangiogenic pathways has precedent in other systems. For example, PDGFR signaling in tumor-associated stromal cells exerts a proangiogenic effect in the tumor microenvironment (36). Furthermore, a recent report revealed that knockout of PDGFR-β in the epicardium inhibits normal development of epicardial coronary arteries (37).

PDGFR-β signaling in the cardiomyocyte may regulate angiogenesis in the heart in response to load-induced stress through several different mechanisms. Recent work has demonstrated that activation of the PI3K and MAPK pathways enhance the angiogenic capacity of cardiomyocytes via a HIF-1α/VEGF-A–dependent mechanism (30). Intriguingly, we observed an increase in levels of phosphorylated Akt and a decrease in levels of phosphorylated p38 in the hearts of *Pdgfrb*^{MerCre} mice prior to TAC compared with levels in hearts of *Pdgfrb*$^{fl/fl}$ mice (Figure 4), although these changes did not achieve statistical significance when quantified by densitometry. Furthermore, we observed significantly decreased phosphorylation of Akt, p38, and ERK1/2 together with significantly decreased expression of HIF-1α and VEGF-A in *Pdgfrb*^{MerCre} mice 14 days after exposure to TAC stress. However, at earlier time points after TAC (day 7), expression of both HIF-1α and VEGF-A were increased in *Pdgfrb*^{MerCre} mice exposed to TAC compared with *Pdgfrb*$^{fl/fl}$ control mice. By this time point, *Pdgfrb*^{MerCre} mice already exhibited cardiac dysfunction along with markedly reduced numbers of blood vessels per cardiomyocyte and functional hypoxia. These observations suggest that the PDGFR-β–dependent angiogenic capacity of cardiomyocytes is *independent* of HIF-1α/VEGF-A expression. Elucidation of the signaling pathways downstream of PDGFR-β that are essential regulators of the PDGFR-β–dependent angiogenic capacity of cardiomyocytes is a goal of our future studies, as is the determination of the precise identity of paracrine factors that mediate the PDGFR-β–dependent paracrine angiogenic capacity of cardiomyocytes. Importantly, cardiomyocyte PDGFR-β signaling may regulate aspects of the cardiac response to pressure overload other than angiogenesis (e.g., substrate utilization) that substantially contribute to heart failure in cardiac-specific PDGFR-β–knockout mice, which we will explore in future studies.

Our findings suggest that therapeutics that augment cardiomyocyte PDGFR signaling in the heart may be a novel strategy for the treatment of cardiac disease in which defective angiogenesis is a contributor to disease pathogenesis. Consistent with this hypothesis are prior studies that demonstrate that administration of PDGF-BB prevents adverse remodeling after experimental myocardial infarction (38, 39). More generally, our findings support the general notion that targeting cardiac

angiogenesis through the PDGF/PDGFR system or via other means may be an effective approach to prevent the progression of multiple forms of heart failure (40), including "nonischemic" cardiomyopathies, in which functional and structural microvascular abnormalities are well described (41).

Our studies were inspired by observations of cardiac toxicity in cancer patients treated with PDGFR inhibitors. Our results provide a mechanistic rationale to aggressively treat hypertension and thus minimize vascular stress as a strategy to prevent heart failure due to anticancer PDGFR inhibitors. Based on our findings, we also speculate that patients with preexisting coronary disease at the macro- or microvascular level may be at increased risk for cardiomyopathy and heart failure associated with these drugs. Confirmation of such findings could provide the basis for a risk stratification tool in cancer patients being considered for treatment with PDGFR inhibitors and could be used to develop strategies to prevent adverse cardiac effects of PDGFR inhibitors.

It is important to note that targets other than PDGFR may be involved in cardiotoxicity due to anticancer PDGFR inhibitors. Both sunitinib and sorafenib can exert substantial off-target effects on other kinases (42), and these can be independent or additive to their effects on cardiomyocyte PDGFR signaling that result in clinical heart failure. Furthermore, cardiotoxicity due to imatinib has been demonstrated to involve Abl kinase (11, 43), while the role of PDGFR signaling in cardiotoxicity due to imatinib is unclear (44). Fundamentally, it is of critical importance to determine the contribution of the inhibitory effects on PDGFR to the clinical cardiac toxicity observed with RTK inhibitors whose targets include PDGFR. Such information will be useful to achieve the goal of designing highly efficacious, novel anticancer agents with minimal cardiotoxicity.

Finally, our studies highlight the opportunities for discovery that can be capitalized upon based upon cardiac toxicity of novel, targeted anticancer agents. Such toxicities may reveal biological pathways whose role in the regulation of cardiovascular physiology were previously unknown, and detailed exploration of such pathways may be useful for developing new, effective treatments for multiple forms of human heart failure.

Methods

Developmental, cardiac-specific PDGFR-β–knockout mice. Mice expressing Cre recombinase driven by the *Nkx2.5* promoter (C57BL/6 background) were crossed with *Pdgfrb*$^{fl/fl}$ mice (129 background) to create *Nkx2.5-Cre:Pdgfrb*$^{fl/fl}$ (*Pdgfrb*$^{Nkx\text{-}Cre}$) mice or littermate control, non–Cre-expressing *Pdgfrb*$^{fl/fl}$ mice (mixed C57BL/6 × 129 background). To study the effects of the *Nkx2.5-Cre* transgene on basal cardiac function in an identical genetic background, we crossed mice expressing Cre recombinase driven by the *Nkx2.5* promoter (C57BL/6 background) with wild-type 129 mice to generate *Nkx2.5-Cre* mice in a mixed C57BL/6 × 129 background. *Nkx2.5-Cre* mice were provided by R.J. Schwartz (Institute of Biosciences and Technology, Houston, Texas, USA). *Pdgfrb*$^{fl/fl}$ mice were provided by P. Soriano (Mount Sinai School of Medicine, New York, New York, USA).

Inducible, cardiac-specific Pdgfrb-knockout mice. To create inducible, cardiac-specific PDGFR-β–knockout mice, we crossed heterozygous α-*MHC-MerCreMer* mice (C57BL/6 background) with *Pdgfrb*$^{fl/fl}$ mice (129 background), resulting in *Pdgfrb*$^{fl/fl}$ mice and α-*MHC-MerCreMer:Pdgfrb*$^{fl/fl}$ (*Pdgfrb*^{MerCre}) mice in a mixed C57BL/6 × 129 background. To study any possible contribution of the α-*MHC-MerCreMer* transgene, we used heterozygous α-*MHC-MerCreMer* mice in a similar, mixed C57BL/6 × 129 background. All groups were treated with 4-hydroxytamoxifen beginning at age 6–8 weeks. 4-Hydroxytamoxifen was administered intraperitoneally at a dosage of 20 mg/kg/d for a total of 5 days. Mice were given 7–10 days of rest after the last dosage of 4-hydroxytamoxifen prior to functional characterization or to exposure to pressure overload–induced stress induced by TAC.

TAC. The University of Texas MD Anderson Cancer Center Institutional Animal Care and Use Committee approved all animal protocols used in this study. Eight- to 12-week-old male mice were used for functional experiments. TAC surgeries were performed based on previously described protocols (45). The sham procedure was similar, except that the aorta was not ligated.

Ultrasound measurement of aortic, carotid, and coronary flows. Carotid velocities were measured 24 hours, 7 days, and 14 days after TAC using a 20-Mhz ultrasound probe connected to a signal processing unit (Indus Instruments) using our previously published protocol (46). CFR was measured as previously described (33). Briefly, the ultrasound probe tip was placed at the left side of the chest of the anesthetized animal and stabilized using a micromanipulator (model MM3-3, World Precision Instruments). Peak coronary velocities were identified, and the probe was fixed in position. Baseline coronary flow was measured at 1.0% isoflurane. As a coronary vasodilator stimulus, the inhaled isoflurane concentration was increased to 2.5%. The coronary vasodilatory properties of isoflurane in general are well described (47), and we have previously validated its use in the measurement of CFR in conjunction with a noninvasive ultrasound technique (33, 48). Ratios of peak velocities at low- (1%) and high-dose (2.5%) isoflurane were reported as CFR.

In vivo myocardial perfusion studies. For myocardial perfusion studies, short- and long-axis echocardiographic images were obtained using the Vevo 770 machine (Visual Sonics). Baseline short-axis images were obtained, followed by injection of a 50-μl bolus containing 1.2×10^7 DEPO Micromarker microbubbles (Visual Sonics) via tail vein. After 12–15 minutes of contrast agent bolus injection, short-axis images were again captured without moving the probe. Global perfusion was only assessable in the anterior and lateral portions of the left ventricle, due to shadowing cast on the septum and posterior aspect of the heart, rendering this data uninterpretable. Quantification of overall perfusion was performed by integrating contrast values obtained from 9 separate measurements from each of at least 3 mice in each group.

Cardiac MRI. Cardiac function in experimental mice was measured by magnetic resonance (MR) scanning using a retrospectively gated imaging method (49). MR scanning experiments were performed using a Bruker 7T MR scanner (BioSpin MRI). Mice were anesthetized using 1%–3% isoflurane in oxygen, and 0.5%–1.5% isoflurane was delivered to maintain anesthesia. During MR scanning, heart rates and respiratory rates were 350–500 beats/minute and 25–40/minute, respectively. Each MR scan included a scout; single-slice sagittal and coronal long-axis cine images of the heart; and a series of axial short-axis cine acquisitions. Sagittal and coronal images were used to establish the cardiac axis and to identify the apex for prescribing short-axis cine slices. Short-axis cine images were used to quantify LV end-diastolic and -systolic volumes. LV volumes, anterior and posterior wall thickness, and LV internal diameter at different phases of the cardiac cycle were measured using ParaVision software (Bruker BioSpin). The total cross-sectional area in the 1-mm-thick short-axis slices (typically 6–8 slices) from apex to base was integrated to calculate ventricular volumes and ejection fractions.

Tissue preparation. We used a previously published method adopted to arrest hearts of inducible mutant mice or controls in diastole and fix them in 10% formalin (50). Five-micrometer sections of formalin-fixed, paraffin-embedded tissue were used for TUNEL assay, H&E staining, Masson's trichrome staining, and immunohistochemistry.

Myocyte cross-sectional area. Horizontal short-axis cut hearts were fixed in 10% buffered formalin solution for 24 hours. Paraffin-embedded hearts were sectioned at 5-mM thickness. All the sections were stained according to previously standard methods. Briefly, sections were deparaffinized, rehydrated, and then incubated for 1 hour with TRITC-labeled lectin

(100 μg/ml; Sigma-Aldrich). Multiple ×400 magnified pictures were captured using a fluorescence microscope (Olympus BX41) from epicardial and endocardial areas of the left ventricle. Myocytes (40–60/heart) that showed round capillaries and clear membrane staining were included in the analysis. The Scion Image (Scion Corp.) program was used to calculate cross-sectional area.

Measurement of microvascular density. We used an antibody directed against CD31 (BD Biosciences) to stain cardiac microvessels. Detection, staining, and counterstaining with hematoxylin was performed using standard methods. For quantification of microvessels, at least 3 random fields (×400) from each of 2 independent sections for each heart assessed were analyzed. To normalize microvessel density to the number of cardiomyocytes present, the same images used to quantify microvessel number were used to count cardiomyocyte nuclei, which were identified based upon their morphologic appearance made visible by counterstaining.

TUNEL assay. TUNEL staining was performed on formalin-fixed, paraffin-embedded tissue using the In Situ Cell Death Detection Kit (Roche Applied Science). Sections were counterstained with DAPI, and apoptotic cells per 10^5 cardiomyocytes were quantified using previously described methods (51).

Tissue hypoxia measurement. To analyze tissue hypoxia 7 and 14 days after TAC, we treated all mice intraperitoneally with 60 mg/kg pimonidazole hydrochloride (Hypoxyprobe, Natural Pharmacia International) 3 hours prior to sacrifice. Immunodetection of Hypoxyprobe binding, indicative of tissue hypoxia, was performed using a previously described method (52). For quantification of cardiac hypoxic area, at least 6 high-magnification (×400) randomly chosen fields from the left ventricle were selected for quantification of immunopositive cells, and the average number of positive staining cells per field was used as an index of tissue hypoxia. Quantification of hypoxic area in hearts of inducible mutant or control mice after TAC was performed by an investigator blinded to the sample identification, using NIH ImageJ software (http://rsbweb.nih.gov/ij/) incorporating standard, grid-based quantitative morphometric techniques (53). For determination of statistical significance between groups at each day, we fit a mixed-effects linear model, with genotype as the fixed effect and animal as the random effect. We used an F-test to determine the significance of differences between genotypes.

Quantitative densitometry. Primary antibodies from Cell Signaling Technology were directed at the following antigens: Akt, phospho-Akt (Ser473), ERK1/2, phospho-ERK1/2 (Thr202/Tyr204), PDGFR-β, JNK, phospho-JNK (Thr183/Tyr185), p38, and phospho-p38 (Thr180/Tyr182). Primary antibodies obtained from Santa Cruz Biotechnology Inc. were directed at the following antigens: VEGF-A, GAPDH, GATA4, and phospho–PDGFR-β (Tyr 1021). Anti–HIF-1α antibody was obtained from Novus Biologicals. Protein bands were quantified via densitometry using Fluorchem 8900 imaging software (Alpha Innotech).

RNA isolation for quantitative RT-PCR and gene expression microarrays. Total RNA was isolated from heart tissues using TRIzol (Invitrogen) reagent using the manufacturer's recommended protocol. RNA integrity was confirmed using an Agilent 2100 Bioanalyzer (Agilent Technologies), with samples run against an RNA ladder of specified molecular weights (Eukaryote Total RNA Nano Series II, Agilent Technologies).

Gene expression microarrays. Mouse genome 430 2.0 array gene chips were purchased from Affymetrix and probed with RNA according to the manufacturer's recommended protocol using a double in vitro transcription method, and data were processed for analysis as previously described (54).

Genotyping by PCR. Genomic DNA was extracted from mouse tails with the RedExtract-N-Amp Tissue PCR Kit (Sigma-Aldrich). Primers were as follows: Nkx2.5-Cre forward, 5′-GGCGTTTTCTGAGCATACCT-3′, and Nkx2.5-Cre reverse, 5′-CTACACCAGAGACGGAAATCCA-3′; internal control forward, 5′-CTAGGCCACAATTGAAAGATCT-3′, and internal control reverse, 5′-GTAGGTGGAAATTCTAGCATCATCC-3′; MerCreMer forward, 5′-ATACCGGAGATCATGCAAGC-3′, and MerCreMer reverse, 5′-AGGTGGACCTGATCATGGGAG-3′; internal control forward, 5′-CTAGGCCACAATTGAAAGATCT-3′, and internal control reverse, 5′-GTAGGTGGAAATTCTAGCATCATCC-3′. To check for the *Pdgfrb* floxed/deleted allele, the forward primer was 5′-GGAAAAGCAGGTTTGTGC-3′, the floxed reverse primer was 5′-TACCAGGAAGGCTTGGGAAG-3′, and the deleted allele reverse primer was 5′-CCAGTTAGTCCACCTATGTTG-3′.

Neonatal murine cardiomyocyte isolation, adenoviral infection, and hypoxia. Neonatal mouse cardiomyocytes were isolated using a commercially available kit from Cellutron (55). Briefly, hearts from 2- to 3-day-old wild-type or *Pdgfrb*$^{fl/fl}$ mice were removed and incubated with digestion medium and then centrifuged to collect the dissociated cells from the medium. Cell cultures were at least 95% pure of cardiomyocytes as determined by flow cytometry after immunostaining of cardiac myosin, a marker of cardiomyocytes. Cells were infected with 25 MOI of adenoviral CMV-GFP or adenoviral CMV-CreGFP (gifts of M.D. Schneider, Imperial College, London, United Kingdom) in growth medium for 48 hours, and then cells were incubated at 37°C with serum-free DMEM F12 (Invitrogen) for 16–24 hours. After 16 hours exposure of cells to hypoxia (1% O_2, 5% CO_2, at 37°C) or normoxia (21% O_2, 5% CO_2, at 37°C), condition medium was collected and stored at –80°C. Cells were collected in TRIzol reagent for RNA isolation.

Endothelial cell proliferation and tube formation assays. HUVECs were cultured in growth medium (5,000 cells/well of 96-well plate). After 3 hours of incubation, growth medium was replaced with condition medium and then incubated for 24 hours. Cells were counted using a Coulter Z series device. The in vitro angiogenesis assay kit was purchased from Millipore, and the assay method was adapted from previous reports (56). Briefly, HUVECs were cultured using endothelial growth medium for 12 hours. HUVECs (5×10^3/well of a 96-well plate) were resuspended in 150 μl condition medium (from 16-hour hypoxia or normoxia) supplemented with 2% heat-inactivated FBS. Resuspended cells were seeded onto the surface of the ECM-coated wells. After 4–8 hours incubation, 3–5 random view fields (×40 magnified) were pictured for each well. Tube length was calculated using ImageJ software.

Statistics. In all figures and within the text, data are presented as mean ± SEM. We tested the data for normality using the Kolmogorov-Smirnov test. To assess statistical significance between groups, we used the unpaired 2-tailed Student's *t* test or, when appropriate, we used the nonparametric, 2-sided Wilcoxon rank-sum test. A *P* value less than 0.05 was considered statistically significant. Changes between multiple groups were calculated using ANOVA, and Tukey's test was then used to test for significant changes between individual groups.

For identification of genes of interest between mutant and control mice over time after TAC using gene expression microarrays, we fit an ANOVA model that accounts for differences due to genotype differences between the 3 time points (day 0, 3, or 7), as well as potential interactions between genotype and day. We used a false discovery rate of 1% to identify genes of interest using this method. To better understand the behavior of the genes found to be differentially expressed by the model (with interaction between treatment and day), we used clustering to group these genes into sets that exhibited similar expression patterns. Gene annotation enrichment analysis of clustered genes was performed using the NIH DAVID annotation tool (http://david.abcc.ncifcrf.gov).

Acknowledgments

We thank T. Finkel (NIH), E.T.H. Yeh (University of Texas MD Anderson Cancer Center), and R. Schwartz (Texas A&M University) for helpful discussions. This work was supported in part by a

Howard Hughes Medical Institute Physician-Scientist Early Career Award (to A.Y. Khakoo), a Physician-Scientist Award from the University of Texas MD Anderson Cancer Center (to A.Y. Khakoo), a Michael and Marriet Cyrus Scholar Award (to A.Y. Khakoo), a postdoctoral fellowship from the American Heart Association (to D. Ai), the NIH (HL076661, HL089792, AG17899 to M.L. Entman), and by the Wanamacker Foundation (to M.L. Entman).

Received for publication September 30, 2009, and accepted in revised form November 18, 2009.

Address correspondence to: Aarif Y. Khakoo, University of Texas MD Anderson Cancer Center, Department of Cardiology, 1515 West Holcombe, Unit 1451, Houston, Texas 77030, USA. Phone: (713) 563-3563; Fax: (713) 563-0462; E-mail: aykhakoo@mdanderson.org.

1. Apte SM, Fan D, Killion JJ, Fidler IJ. Targeting the platelet-derived growth factor receptor in antivascular therapy for human ovarian carcinoma. *Clin Cancer Res*. 2004;10(3):897–908.
2. Ostman A, Heldin CH. Involvement of platelet-derived growth factor in disease: development of specific antagonists. *Adv Cancer Res*. 2001;80:1–38.
3. Sundberg C, Ljungstrom M, Lindmark G, Gerdin B, Rubin K. Microvascular pericytes express platelet-derived growth factor-beta receptors in human healing wounds and colorectal adenocarcinoma. *Am J Pathol*. 1993;143(5):1377–1388.
4. Uehara H, et al. Effects of blocking platelet-derived growth factor-receptor signaling in a mouse model of experimental prostate cancer bone metastases. *J Natl Cancer Inst*. 2003;95(6):458–470.
5. Escudier B, et al. Sorafenib in advanced clear-cell renal-cell carcinoma. *N Engl J Med*. 2007; 356(2):125–134.
6. Peggs K, Mackinnon S. Imatinib mesylate — the new gold standard for treatment of chronic myeloid leukemia. *N Engl J Med*. 2003;348(11):1048–1050.
7. Motzer RJ, et al. Sunitinib in patients with metastatic renal cell carcinoma. *JAMA*. 2006; 295(21):2516–2524.
8. Chu TF, et al. Cardiotoxicity associated with tyrosine kinase inhibitor sunitinib. *Lancet*. 2007; 370(9604):2011–2019.
9. Khakoo AY, et al. Heart failure associated with sunitinib malate: a multitargeted receptor tyrosine kinase inhibitor. *Cancer*. 2008;112(11):2500–2508.
10. Schmidinger M, et al. Cardiac toxicity of sunitinib and sorafenib in patients with metastatic renal cell carcinoma. *J Clin Oncol*. 2008;26(32):5204–5212.
11. Kerkela R, et al. Cardiotoxicity of the cancer therapeutic agent imatinib mesylate. *Nat Med*. 2006; 12(8):908–916.
12. Atallah E, Durand JB, Kantarjian H, Cortes J. Congestive heart failure is a rare event in patients receiving imatinib therapy. *Blood*. 2007;110(4):1233–1237.
13. Wu S, Chen JJ, Kudelka A, Lu J, Zhu X. Incidence and risk of hypertension with sorafenib in patients with cancer: a systematic review and meta-analysis. *Lancet Oncol*. 2008;9(2):117–123.
14. Moses KA, DeMayo F, Braun RM, Reecy JL, Schwartz RJ. Embryonic expression of an Nkx2-5/Cre gene using ROSA26 reporter mice. *Genesis*. 2001; 31(4):176–180.
15. Schmahl J, Rizzolo K, Soriano P. The PDGF signaling pathway controls multiple steroid-producing lineages. *Genes Dev*. 2008;22(23):3255–3267.
16. Leveen P, Pekny M, Gebre-Medhin S, Swolin B, Larsson E, Betsholtz C. Mice deficient for PDGF B show renal, cardiovascular, and hematological abnormalities. *Genes Dev*. 1994;8(16):1875–1887.
17. Price RL, Thielen TE, Borg TK, Terracio L. Cardiac defects associated with the absence of the platelet-derived growth factor alpha receptor in the patch mouse. *Microsc Microanal*. 2001;7(1):56–65.
18. Zhang YM, et al. Targeted deletion of ROCK1 protects the heart against pressure overload by inhibiting reactive fibrosis. *FASEB J*. 2006;20(7):916–925.
19. Sohal DS, et al. Temporally regulated and tissue-specific gene manipulations in the adult and embryonic heart using a tamoxifen-inducible Cre protein. *Circ Res*. 2001;89(1):20–25.
20. He Q, Wang D, Yang XP, Carretero OA, LaPointe MC. Inducible regulation of human brain natriuretic peptide promoter in transgenic mice. *Am J Physiol Heart Circ Physiol*. 2001;280(1):H368–H376.
21. Heldin CH, Ostman A, Ronnstrand L. Signal transduction via platelet-derived growth factor receptors. *Biochim Biophys Acta*. 1998;1378(1):F79–F113.
22. Dorn GW II, Force T. Protein kinase cascades in the regulation of cardiac hypertrophy. *J Clin Invest*. 2005;115(3):527–537.
23. Bassi R, Heads R, Marber MS, Clark JE. Targeting p38-MAPK in the ischaemic heart: kill or cure? *Curr Opin Pharmacol*. 2008;8(2):141–146.
24. Purcell NH, et al. Genetic inhibition of cardiac ERK1/2 promotes stress-induced apoptosis and heart failure but has no effect on hypertrophy in vivo. *Proc Natl Acad Sci U S A*. 2007;104(35):14074–14079.
25. Eyries M, et al. Hypoxia-induced apelin expression regulates endothelial cell proliferation and regenerative angiogenesis. *Circ Res*. 2008;103(4):432–440.
26. Chen JX, Zeng H, Lawrence ML, Blackwell TS, Meyrick B. Angiopoietin-1-induced angiogenesis is modulated by endothelial NADPH oxidase. *Am J Physiol Heart Circ Physiol*. 2006;291(4):H1563–H1572.
27. van Hinsbergh VW, Koolwijk P. Endothelial sprouting and angiogenesis: matrix metalloproteinases in the lead. *Cardiovasc Res*. 2008;78(2):203–212.
28. Heineke J, et al. Cardiomyocyte GATA4 functions as a stress-responsive regulator of angiogenesis in the murine heart. *J Clin Invest*. 2007;117(11):3198–3210.
29. Sano M, et al. p53-induced inhibition of Hif-1 causes cardiac dysfunction during pressure overload. *Nature*. 2007;446(7134):444–448.
30. Walsh K, Shiojima I. Cardiac growth and angiogenesis coordinated by intertissue interactions. *J Clin Invest*. 2007;117(11):3176–3179.
31. Saraste A, Kyto V, Saraste M, Vuorinen T, Hartiala J, Saukko P. Coronary flow reserve and heart failure in experimental coxsackievirus myocarditis. A transthoracic Doppler echocardiography study. *Am J Physiol Heart Circ Physiol*. 2006;291(2):H871–H875.
32. Lucarini AR, Picano E, Salvetti A. Coronary microvascular disease in hypertensives. *Clin Exp Hypertens A*. 1992;14(1–2):55–66.
33. Hartley CJ, et al. Doppler estimation of reduced coronary flow reserve in mice with pressure overload cardiac hypertrophy. *Ultrasound Med Biol*. 2008;34(6):892–901.
34. Kaufmann BA, et al. High-resolution myocardial perfusion imaging in mice with high-frequency echocardiographic detection of a depot contrast agent. *J Am Soc Echocardiogr*. 2007;20(2):136–143.
35. Choi YH, et al. Myocardial hypertrophy overrides the angiogenic response to hypoxia. *PLoS ONE*. 2008;3(12):e4042.
36. Pietras K, Pahler J, Bergers G, Hanahan D. Functions of paracrine PDGF signaling in the proangiogenic tumor stroma revealed by pharmacological targeting. *PLoS Med*. 2008;5(1):e19.
37. Mellgren AM, et al. Platelet-derived growth factor receptor beta signaling is required for efficient epicardial cell migration and development of two distinct coronary vascular smooth muscle cell populations. *Circ Res*. 2008;103(12):1393–1401.
38. Hsieh PC, Davis ME, Gannon J, MacGillivray C, Lee RT. Controlled delivery of PDGF-BB for myocardial protection using injectable self-assembling peptide nanofibers. *J Clin Invest*. 2006;116(1):237–248.
39. Hsieh PC, MacGillivray C, Gannon J, Cruz FU, Lee RT. Local controlled intramyocardial delivery of platelet-derived growth factor improves postinfarction ventricular function without pulmonary toxicity. *Circulation*. 2006;114(7):637–644.
40. Gavin JB, Maxwell L, Edgar SG. Microvascular involvement in cardiac pathology. *J Mol Cell Cardiol*. 1998;30(12):2531–2540.
41. Tsagalou EP, et al. Depressed coronary flow reserve is associated with decreased myocardial capillary density in patients with heart failure due to idiopathic dilated cardiomyopathy. *J Am Coll Cardiol*. 2008; 52(17):1391–1398.
42. Force T, Krause DS, Van Etten RA. Molecular mechanisms of cardiotoxicity of tyrosine kinase inhibition. *Nat Rev Cancer*. 2007;7(5):332–344.
43. Demetri GD. Structural reengineering of imatinib to decrease cardiac risk in cancer therapy. *J Clin Invest*. 2007;117(12):3650–3653.
44. Chintalgattu V, Patel SS, Khakoo AY. Cardiovascular effects of tyrosine kinase inhibitors used for gastrointestinal stromal tumors. *Hematol Oncol Clin North Am*. 2009;23(1):97–107, viii–ix.
45. Li YH, et al. Effect of age on peripheral vascular response to transverse aortic banding in mice. *J Gerontol A Biol Sci Med Sci*. 2003;58(10):B895–B899.
46. Li YH, Reddy AK, Taffet GE, Michael LH, Entman ML, Hartley CJ. Doppler evaluation of peripheral vascular adaptations to transverse aortic banding in mice. *Ultrasound Med Biol*. 2003;29(9):1281–1289.
47. Zhou X, Abboud W, Manabat NC, Salem MR, Crystal GJ. Isoflurane-induced dilation of porcine coronary arterioles is mediated by ATP-sensitive potassium channels. *Anesthesiology*. 1998;89(1):182–189.
48. Hartley CJ, et al. Effects of isoflurane on coronary blood flow velocity in young, old and ApoE(–/–) mice measured by Doppler ultrasound. *Ultrasound Med Biol*. 2007;33(4):512–521.
49. Crowe ME, et al. Automated rectilinear self-gated cardiac cine imaging. *Magn Reson Med*. 2004; 52(4):782–788.
50. Michael LH, et al. Myocardial infarction and remodeling in mice: effect of reperfusion. *Am J Physiol*. 1999;277(2 Pt 2):H660–H668.
51. Chang J, et al. Activation of Rho-associated coiled-coil protein kinase 1 (ROCK-1) by caspase-3 cleavage plays an essential role in cardiac myocyte apoptosis. *Proc Natl Acad Sci U S A*. 2006;103(39):14495–14500.
52. Kleiter MM, et al. A comparison of oral and intravenous pimonidazole in canine tumors using intravenous CCI-103F as a control hypoxia marker. *Int J Radiat Oncol Biol Phys*. 2006;64(2):592–602.
53. Mouton PR. *Principles and Practices of Unbiased Stereology: An Introduction for Bioscientists*. Baltimore, MD: Johns Hopkins University Press; 2002.
54. Gold D, et al. A comparative analysis of data generated using two different target preparation methods for hybridization to high-density oligonucleotide microarrays. *BMC Genomics*. 2004;5(1):2.
55. Vallentin A, Mochly-Rosen D. RBCK1, a protein kinase CβI (PKCβI)-interacting protein, regulates PKCβ-dependent function. *J Biol Chem*. 2007; 282(3):1650–1657.
56. Chintalgattu V, Harris GS, Akula SM, Katwa LC. PPAR-gamma agonists induce the expression of VEGF and its receptors in cultured cardiac myofibroblasts. *Cardiovasc Res*. 2007;74(1):140–150.